NASA Technical Memorandum 4083

Analysis of an Unswept Propfan Blade With a Semiempirical Dynamic Stall Model

T. S. R. Reddy
The University of Toledo
Toledo, Ohio

K. R. V. Kaza
Lewis Research Center
Cleveland, Ohio

National Aeronautics
and Space Administration

**Scientific and Technical
Information Division**

1989

Summary

The time-history response of a propfan wind-tunnel model with dynamic stall was studied analytically. The response obtained from the analysis was compared with available experimental data. The governing equations of motion were formulated in terms of blade normal modes calculated using the COSMIC–NASTRAN computer code. The response analysis considered the blade plunging and pitching motions. The lift, drag, and moment coefficients for angles of attack below the static stall angle were obtained from a quasi-steady theory. For angles above static stall angles, a semiempirical dynamic stall model based on a correction to the angle of attack was used to obtain lift, drag, and moment coefficients. Using these coefficients, the aerodynamic forces were calculated at a selected number of strips, and integrated to obtain the total generalized forces. The combined momentum—blade element theory was used to calculate the induced velocity.

The semiempirical stall model predicted a limit cycle oscillation near the setting angle at which large vibratory stresses were observed in an experiment. The predicted mode and frequency of oscillation also agreed with those measured in the experiment near this setting angle. The results also correlated well with the other published data that used a semiempirical dynamic stall model based on a synthesized procedure.

Introduction

Modern propeller designs are being considered to power transport aircraft at high subsonic speeds. These new propeller designs, called propfans, are expected to result in significant savings in fuel consumption. Figure 1 shows the characteristics of a typical propfan. Compared to a conventional propeller, the number of blades and width of the blade chord of the propfan are increased to provide a high disk loading. The blades are thin to increase the drag divergence Mach number and are swept to reduce the local effective Mach number and noise. Flutter analysis of these propfans is needed to determine the critical (flutter) speed below which the aircraft has to operate to avoid catastrophic blade failure. A response analysis is needed to determine the stresses and fatigue life of the blades. The aeroelastic response and flutter analyses of propfans are ongoing research efforts at NASA Lewis Research Center. Flutter analysis methods and experimental flutter results for propfans at low angles of attack (classical flutter) are described in references 1 to 4. The analyses include the effects of number of blades (cascade effects), blade pitch angle, blade sweep, and mistuning.

However, under static or low-speed conditions, the propfan sections may operate at high angles of attack and have the potential to stall flutter, which is triggered by separated flow during part of every cycle of oscillation. Stall-flutter speeds are very low compared to classical flutter speeds, and the resulting vibratory stresses can cause fatigue failure of the propfan. Hence, avoiding stall flutter is a critical design condition, and analysis of stall flutter and prediction of unsteady forces due to flow separation are critical research needs.

In steady flow, above a certain critical angle of attack, the flow over an airfoil breaks down—a phenomenon called static stall (flow separation). In the case of an oscillating airfoil this stall phenomenon is referred to as dynamic stall. There has been considerable research to understand dynamic stall and its effects (refs. 5 and 6). The three important effects of dynamic stall are shown schematically in figure 2, and are summarized as follows:

(1) Stall delay—An airfoil with a positive rate of angle of attack (upstroke) stalls at an angle of attack greater than the

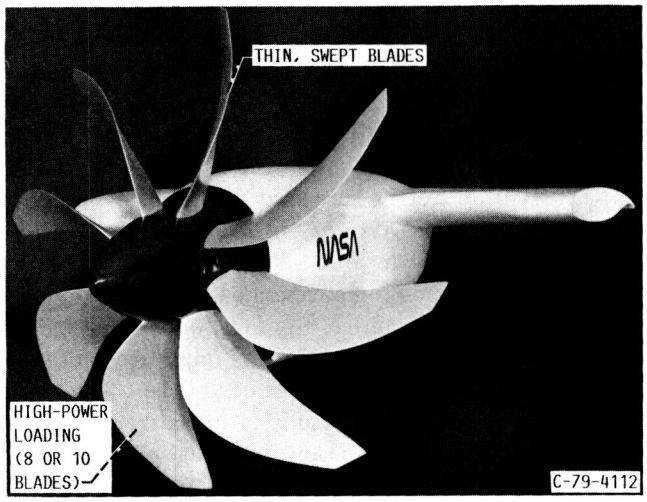

Figure 1.—Wind tunnel model of a propfan.

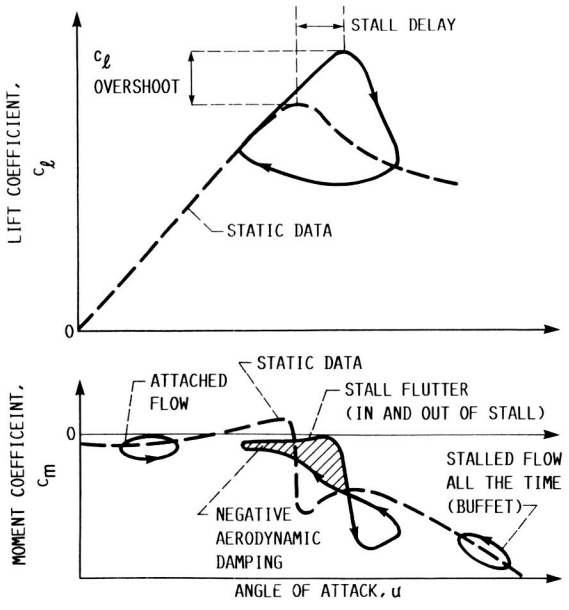

Figure 2.—Three unsteady effects of dynamic stall.

static stall angle. This means that an oscillating airfoil can reach higher angles of attack than a static airfoil can reach before the flow separates. The stall recovery (reattachment) during a negative rate of angle of attack (downstroke) generally occurs at an angle less than the static stall angle.

(2) Overshoot of the forces and moments—The vibratory forces and moments are considerably higher than those for the static counterparts. This affects stresses and the fatigue life of the propfan.

(3) Negative aerodynamic damping—The dynamic stall events—namely, separation of the flow, formation of the vortex, movement of the vortex, and reattachment—take a finite time to develop. However, once the flow is separated, the dynamic stall events introduce two important physical consequences. The first is the hysteresis produced by the lag and asymmetry of the airloads with respect to the motion of the body. This is in contrast to the quasi-steady case where no hysteresis is produced since the flow field adjusts immediately to each change in angle of attack. The second consequence is aerodynamic damping, which is related to the net work done over a complete cycle of oscillation. If this damping is negative, the airfoil extracts energy from the airstream. This is the condition of flutter. Stall flutter, arising from this negative damping, tends to occur when the airfoil is oscillating in and out of stall.

Attempts to predict these effects due to dynamic stall follow two approaches, one theoretical, and the other based on experimental data (semiempirical) (refs. 5 to 7). The theoretical approaches attempt to solve the fluid mechanics equations in their fundamental form by numerical techniques with varying degrees of simplifications and assumptions. These include evaluating the flow field using the Navier-Stokes equations, the discrete vortex methods, and the coupled viscous-inviscid methods (zonal methods). These methods, in addition to their limited development, require significant computer time and therefore are not suitable for routine aeroelastic analysis.

The semiempirical models attempt to simulate the gross features of stall. The various parameters in these models are determined by fitting theory to experimental data obtained from oscillating airfoil tests. These models gained much interest for the following reasons: (1) They use static airfoil data (lift, drag, and moment coefficients for different angles of attack at different Mach numbers) with a correction for dynamic (unsteady) effects. This is advantageous because static airfoil data can be easily generated and automatically include the effects of Reynolds number, Mach number, and airfoil shape; and (2) the models take less computer time, so they can be used in a routine aeroelastic analysis.

The empirical parameters used in these semiempirical models are usually based on the experimental data obtained from airfoils oscillating in pitch about quarter chord. However, an arbitrary motion includes both pitch and plunge motions. So stall modeling should include separate plunge motion terms in the identification of the empirical parameters. Many of the existing semiempirical models do not take into account the distinction between pitch and plunge motions. In order to use the existing empirical models in an aeroelastic analysis where the unsteady motion consists of both plunging and pitching, an equivalent angle of attack based on both the pitch and plunge motions of the airfoil is calculated and used.

The objective of the present effort is to predict the stall-flutter behavior of a propfan wind-tunnel model using a semiempirical dynamic stall model. Wind-tunnel experiments of the SR-2 propfan (SR for single rotation and 2 for design number 2) have indicated that it is prone to stall flutter at static thrust (zero wind speed) conditions (refs. 8 and 9). The buildup of high stresses at noncritical speeds during the experiment is taken as the condition indicating stall flutter. The experiments showed that the stall flutter response occurred in the third mode (first torsion). In reference 5, three semiempirical dynamic stall models are compared with respect to lift, drag, and moment coefficients by applying them to airfoils oscillating sinusoidally. The three models are the Gormont model (ref. 10), the Gangwani model (ref. 11), and the ONERA model (ref. 12). These are referred to in reference 5 as models A, B, and C, respectively. Of these models, the Gormont model requires only one empirical stall parameter, which is given as a function of Mach number and airfoil thickness to chord ratio. The Gangwani and ONERA models require a large number of dynamic stall parameters that depend on the airfoil section used. These parameters are not available for propfan airfoil sections (NACA 16 series). Therefore, in the present study, the Gormont model is used to analyze the SR-2 propfan wind-tunnel model.

Reference 8 presents analytical stall-flutter results for the SR-2 propfan based on a linear structural model and a linear aerodynamic model which are based on the theory presented in reference 13. The results predict the mode and the blade setting angle for which stall flutter occurred in tests. However, this analysis is insufficient since the present problem is nonlinear both structurally (because of large deflections) and aerodynamically (because of high angle of attack and separated flow). The analysis of reference 8 only predicts the onset of stall flutter; it does not calculate the limit amplitude response of the propfan blade. An analytical model of the SR-2 propfan for stall flutter also is presented in reference 14. This analysis uses a nonlinear beam structural model and the Gangwani dynamic stall model (model B). The dynamic stall data of an NLR-1 airfoil (ref. 11) are used since dynamic stall data for the NACA 16 series are not available. The analysis qualitatively predicts the stall-flutter behavior of the SR-2 propfan blade at static thrust conditions.

The present analysis differs from that of references 8 and 14 in that a nonlinear, large-deflection finite element formulation is used in modeling the structural behavior of the propfan. This formulation results in more accurate representation of the deformed steady and modal blade geometry than is obtained with a beam formulation. The present formulation is also more suitable for application to other swept

propfans made of composite materials. The model-A dynamic stall model, where Mach number and thickness effects are accounted for in the stall model, is used for aerodynamic calculations. This simulates the approximate dynamic stall effects of NACA 16 series airfoils, rather than the NLR–1 airfoil dynamic stall effects used in reference 14. In contrast to the linear structural and aerodynamic model of reference 8, the present model includes nonlinear structural and aerodynamic forces and dynamic stall effects. The numerical study is performed for a single blade by neglecting structural and aerodynamic coupling between blades. The results are compared with the theoretical results of reference 14 and with experimental data of reference 8.

In the following sections, first the governing equations of motion are given, and then the results and discussion of a numerical stall-flutter study with the computer code developed are presented. As an aid to the reader, a symbols list is given in appendix A.

Aeroelastic Equations of Motion

Coordinate Systems

Three orthogonal coordinate systems used in the formulation are illustrated in figure 3(a). The axis system X_I, Y_I, Z_I is fixed in space and defines an inertial system. The X_I axis is along the hub rotation axis and the Y_I axis is along the blade pitch change axis, with the blade in an undeflected position. The axis system X_B, Y_B, Z_B, called the basic coordinate system, is attached to the propfan blade. The propfan is rotating about the X_B axis with an angular velocity Ω and the Y_B axis is along the blade pitch change axis. Thus the X_B, Y_B, Z_B system is obtained by rotating the X_I, Y_I, Z_I system by an angle $\psi = \Omega t$. The unit vectors along X_B, Y_B, and Z_B are given by $\hat{i}$, $\hat{j}$, and $\hat{k}$, respectively. The transformation from the basic coordinate system X_B, Y_B, Z_B to the inertial coordinate system X_I, Y_I, Z_I is given by

$$\begin{Bmatrix} X \\ Y \\ Z \end{Bmatrix}_I = \begin{bmatrix} 1 & 0 & 0 \\ 0 & \cos(\psi) & -\sin(\psi) \\ 0 & \sin(\psi) & \cos(\psi) \end{bmatrix} \begin{Bmatrix} X \\ Y \\ Z \end{Bmatrix}_B \tag{1a}$$

where

$$\psi = \Omega t$$

or

$$\{X\}_I = [T_1]\{X\}_B \tag{1b}$$

The axis system X_ℓ, Y_ℓ, Z_ℓ defines a local coordinate system at any point on a chosen blade reference axis. The X_ℓ axis is

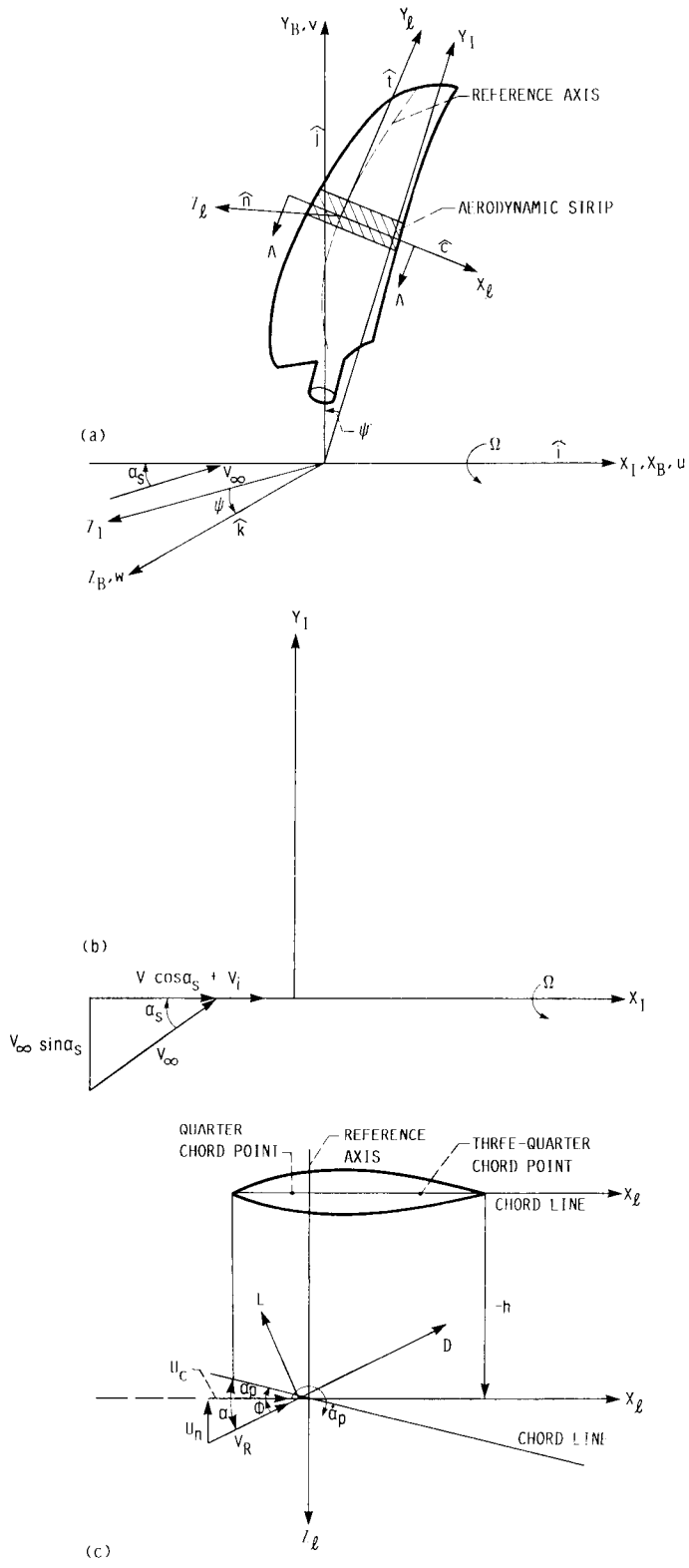

(a) Three orthogonal coordinate systems.
(b) Free-stream and induced velocity.
(c) Definition of pitching and plunging motions, section A–A.

Figure 3.—Blade coordinate system.

normal to the reference axis and is positive from leading edge to trailing edge; the Y_ℓ axis is along the tangent to the reference axis at the point under consideration and is positive in the direction of propfan root to tip; and the Z_ℓ axis is perpendicular to both X_ℓ and Y_ℓ and is positive in the direction of a right-handed system. The unit vectors along X_ℓ, Y_ℓ, and Z_ℓ are given respectively by $\hat{c}$, $\hat{t}$, and $\hat{n}$. The relation between the basic coordinate system and local coordinate system can be written as

$$\{X\}_B = [T_2]\{X\}_\ell \tag{2}$$

where $[T_2]$, the transformation matrix, can be calculated from the geometry of the propfan blade. A brief explanation of the calculation procedure is given in appendix B. It should be noted that the transformation matrix $[T_2]$ varies from point to point on the reference axis. In general, the blade deforms to a steady-state position about which the perturbation (vibratory) motion is superimposed. In the present analysis the steady displacements are assumed to be caused by the centrifugal forces only. The local coordinate system and the transformation matrix, $[T_2]$, are calculated with reference to the steady-state position of the blade. This means that the aeroelastic analysis presented in this report is, in fact, a quasi-linear analysis, where a linearized structural model is coupled with a nonlinear aerodynamic model.

Equations of Motion

The governing equations of motion for the propfan are formulated in terms of normal modes. The blade is considered to be fixed at one end and free at the other. The normal modes of the rotating propfan can be obtained from a finite element analysis program that includes a geometric nonlinear analysis to account for the large deflections and rotational effects of the propfan. The finite element analysis results in a large number of nonlinear governing equations of motion that are computationally expensive to solve. However, the governing equations of motion can be linearized, which permits simplification of the equations; they can be expressed as a superposition of normal modes, which reduces the large number of equations. The formation, linearization, and conversion of the governing equations of motion into equations in normal coordinates for a propfan are described in reference 3. In the present report only the calculation of generalized aerodynamic forces is presented. The final governing equations of motion for each mode can be written as

$$\ddot{q}_i + 2\zeta_i \omega \dot{q}_i + \omega_i^2 q_i = \frac{Q_i}{m_i} \qquad i = 1,2,\ldots,NM \tag{3}$$

where m_i is the ith generalized mass, ω_i is the circular frequency in the ith normal mode, ζ_i is the critical damping (structural) ratio in the ith mode, Q_i is the ith generalized force including aerodynamic contributions, NM is the number of normal modes used in the analysis, and q_i is the ith normal coordinate, which is a function of time.

Generalized Aerodynamic Forces

In the present study, strip theory is used to calculate the generalized aerodynamic forces on the blade. The blade is divided into a series of discrete aerodynamic strips that are normal to an arbitrary reference line (reference axis). One of these strips is shown in figure 3(a). Each strip has two motions: (1) plunging and (2) pitching about the arbitrary reference line. The generalized forces calculated at each strip along the radius of the blade are integrated to obtain the total generalized force (Q_i) in each mode. The two-dimensional, incompressible, quasi-steady theory is used in calculating the velocities and forces. Stall effects are included via a semiempirical dynamic stall model. The noncirculatory lift and moment associated with apparent mass forces are neglected. The classical combined momentum—blade element theory, as given in appendix C, is used to calculate the steady induced velocity. It is also assumed that the spanwise velocity component (along the Y_ℓ axis) does not contribute to the aerodynamic loads.

With the above assumptions, the calculation of the aerodynamic part of Q_i involves the calculation of (1) the relative velocity at a point on the reference line of the airfoil and the angle of attack, (2) the unsteady force coefficients, and (3) the generalized aerodynamic forces. These calculations follow.

(1) Relative velocity and angle of attack calculation.—To calculate the aerodynamic loads, one must calculate the velocity of a point on the reference axis of the blade relative to the air velocity. This velocity is calculated in the blade local coordinate system. The contributions to the relative velocity are (a) oncoming wind and induced velocity and (b) velocity due to blade rotation and vibratory motion.

(a) Wind velocity and induced velocity (fig. 3(b)): The oncoming air makes an angle, α_s, with respect to the normal of the disk plane. Therefore the components in the X_I direction and in the plane of the disk are $V_\infty \cos\alpha_s$ and $V_\infty \sin\alpha_s$. Let the steady induced velocity be given by V_i, which acts in the positive direction of X_I. Then, $\{V\}_a$, the velocity contribution from airflow in the local coordinate system (fig. 3(b)), is given by

$$\{V\}_a = [T_2]^T[T_1]^T \begin{Bmatrix} V_\infty \cos\alpha_s + V_i \\ V_\infty \sin\alpha_s \\ 0 \end{Bmatrix} \tag{4}$$

(b) Velocity contribution from blade motion and rotation: The propfan is rotating about the X_B axis. Let u_0, v_0, and w_0 be the steady displacements due to centrifugal loads, and u, v, and w be the unsteady (perturbed) displacements due to

Appendix D
Effect of Airfoil Static Data Variation on the Dynamic Stall Response

To understand the effect of airfoil static data above stall on the stall-flutter response, one can make calculations with prescribed static data above stall, and the variation in response can be studied. However, for a response study, c_ℓ, c_m, and c_d cannot be varied independently since they are interr[illegible] However, dynamic stall loops (dynamic lift, moment, and drag versus angle of attack) can be obtained with independent variation of static lift, drag, and moment coefficients above stall, and some inference can be drawn. In stall flutter, the negative aerodynamic damping is mostly from the dynamic moment loop. So in the present study the static $c_{mc/4}$ is varied and the dynamic moment loops are studied. Three cases are studied as shown below and in figure 16.

Case-A Moment Coefficient

This case is a curve-fitted expression for the static moment data given in the G400PROP program (ref. 14) at the 75-percent-radius location for a Mach number of 0.7,

$$c_{mc/4} = -0.035 - 0.003^*\alpha \qquad \text{for } \alpha < 6°$$

$$c_{mc/4} = -0.053 - 0.024^*(\alpha - 6.0) \qquad \text{for } 6° < \alpha < 10°$$

$$c_{cm/4} = -0.149 - 0.0085^*(\alpha - 10) \qquad \text{for } \alpha > 10°$$

Case-B Moment Coefficient

$$c_{mc/4} = -0.553 - 0.015(\alpha - 6) \qquad \text{for } \alpha > 6°$$

Case-C Moment Coefficient

$$c_{mc/4} = -0.553 - 0.010(\alpha - 6) \qquad \text{for } \alpha > 6°$$

Figure 17 shows the dynamic $c_{mc/4}$ loops obtained with static-stall moment data assumed as above. The angle-of-attack variation is given by $\alpha = 5° + 3° \sin(\omega t)$ at a reduced frequency of 0.05 and for a Mach number of 0.7. The dynamic loops are indicative of the energy transfer from the flow to the structure. In figure 17, the dynamic loop obtained with case-A static data shows a large hysteresis loop above stall, which means that negative work is being done on the structure. This may lead to a net negative damping at certain flow conditions. The area of the loop reduces by about half with case-B assumed static data. With the case-C assumed static data no negative loop is obtained, indicating there is no negative work on the structure. This shows that inaccurate static data above stall can lead to positive or negative damping, leading to stable or unstable response.

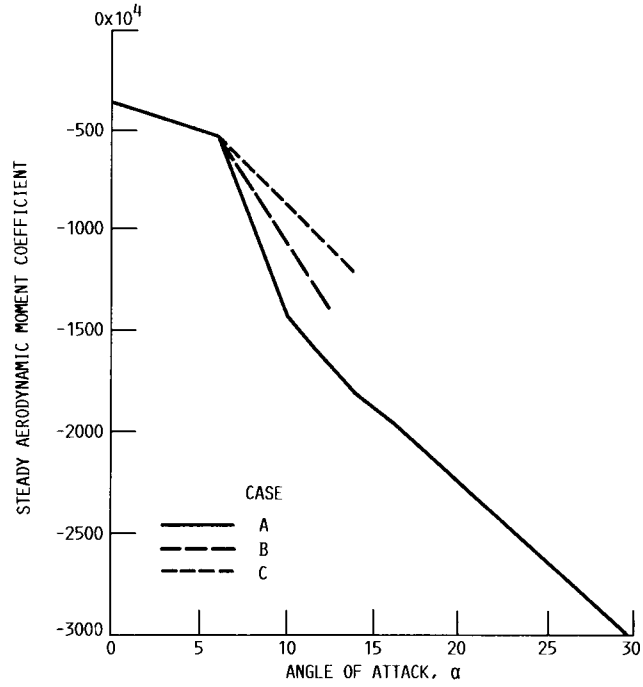

Figure 16.—Variation of static moment coefficient with angle of attack.

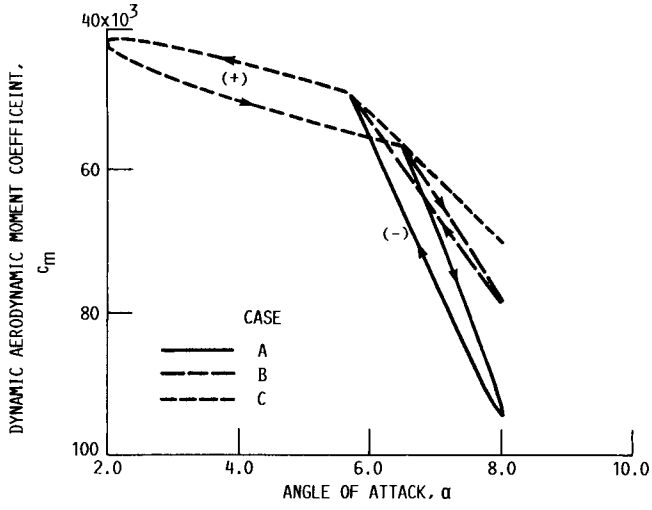

Figure 17.—Variation of dynamic moment coefficient with assumed static moment coefficient at Mach 0.7 and reduced frequency, k, of 0.05; $\alpha = 5 + 3 \sin ks$; model A dynamic stall.

vibration of any point on the reference axis, in the X_B, Y_B, and Z_B directions, respectively; u_0, v_0, and w_0 are functions of x, y, and z, and u, v, and w are functions of x, y, z, and t, where x, y, and z are coordinates of the point in the basic (rotating) coordinate system X_B,Y_B,Z_B. Then the absolute velocity $d\bar{r}/dt$ of a point x,y,z is given by

$$\frac{d\bar{r}}{dt} = \dot{\bar{r}} + \bar{\omega} \times \bar{r} \tag{5}$$

where $\bar{\omega}$ is the angular velocity of the X_B,Y_B,Z_B coordinate system and is given by

$$\bar{\omega} = \Omega i \tag{6}$$

where Ω is the rotational speed in rad/sec, and $\bar{r}$, the position vector of the point under consideration, is given by

$$\begin{aligned}\bar{r} &= (x + u_0)\hat{i} + (y + v_0)\hat{j} + (z+w_0)\hat{k} + u\hat{i} + v\hat{j} + w\hat{k} \\ &= \bar{r}_s + u\hat{i} + v\hat{j} + w\hat{k}\end{aligned} \tag{7}$$

where $\bar{r}_s$ represents the position vector of the point under consideration including steady displacements due to centrifugal loads.

The transformation of $d\bar{r}/dt$, that is, the velocity of the point x,y,z, into the local coordinate system, is given by

$$\begin{aligned}\{V\}_b = [T_2]^T\left(\frac{d\bar{r}}{dt}\right) &= [T_2]^T(\dot{\bar{r}} + \bar{\omega} \times \bar{r}) \\ &= [T_2]^T\dot{\bar{r}} + [T_2]^T(\bar{\omega} \times \bar{r}) \\ &= \{V\}_m + \{V\}_{\text{rot}}\end{aligned} \tag{8}$$

where subscripts b, m, and rot indicate blade, from-blade vibratory motion, and from-blade rotation (Ω), respectively. In the present analysis, the components of $\{V\}_b$ are calculated for points on the reference axis (reference line).

Then the relative velocity of any point on the reference axis is given by (eqs. (4) to (8))

$$\{V\}_{\text{rel}} = \{V\}_a - \{V\}_b = \{V\}_a - \{V\}_{\text{rot}} - \{V\}_m \tag{9}$$

$$\{V\}_{\text{rel}} = \begin{Bmatrix} V_1 \\ V_2 \\ V_3 \end{Bmatrix} - \{V\}_m \tag{10a}$$

where

$$(V_1,V_2,V_3) = \{V\}_a - \{V\}_{\text{rot}} \tag{10b}$$

The components of $\{V\}_m$ are contributions from the blade motion to the velocities in the local coordinate system and are calculated as follows. First, for each strip, the modal deflections are transformed into plunge h_i and pitch α_i motions about the reference axis in the X_ℓ,Y_ℓ,Z_ℓ system. The plunge and pitch motions are shown in figure 3(c), with plunging motion being positive in the negative Z_ℓ direction, and pitching motion being positive for the leading-edge-up (nose-up) position. Reference 3 describes the procedure of obtaining h_i and α_i (for each mode) from the general vibratory motion. Then the total plunging displacement h of a point on the reference axis and the pitching displacement α_p about the reference axis, for each strip, can be expressed as sum of the contributions from various normal modes:

$$\begin{aligned} h &= \sum_{i=1}^{NM} h_i q_i \\ \alpha_p &= \sum_{i=1}^{NM} \alpha_i q_i \end{aligned} \tag{11}$$

where h_i and α_i are the contributions to total plunge and pitch motions, respectively, from the ith modal deflections, and NM is number of normal modes. Then, neglecting all other components, the velocity due to blade motion of a point on the reference axis is given by

$$\{V\}_m = \begin{Bmatrix} 0 \\ 0 \\ -\dot{h} \end{Bmatrix} \tag{12}$$

and the rotation of the strip is given by α_p.

The velocity vector $\{V\}_{\text{rel}}$ (eq. (9)) can be written in terms of U_c, U_t, and U_n—the chordwise, tangential (spanwise), and normal components of velocity of the airfoil—as shown in figure 3(c):

$$\{V\}_{\text{rel}} = U_c\hat{c} + U_t\hat{t} - U_n\hat{n} \tag{13}$$

The next step is to calculate the angle of attack of the strip in terms of U_c, U_t, and U_n. But, it is well known that the lift of the airfoil is proportional to the downwash velocity of the three-quarter chord point on the airfoil. Since U_n is the velocity perpendicular to the chord at the reference point, the sectional angle of attack can be written as

$$\alpha = \tan^{-1}\left(\frac{-U_n + d\dot{\alpha}_p}{U_c}\right) + \alpha_p = \phi + \alpha_p \tag{14}$$

$$\left.\begin{aligned} F_{X_\ell} &= -L\sin(\phi) + D\cos(\phi) \\ F_{Z_\ell} &= -L\cos(\phi) - D\sin(\phi) \\ M_{\text{ref}} &= M_a + La \end{aligned}\right\} \qquad (20)$$

where M_{ref} refers to the moment about the reference axis and a is the distance between the reference axis and the quarter chord (positive for reference axis aft of quarter chord). Then the generalized force at the jth strip is given by

$$f_{ij} = [h_i(y_j)F_{Z_\ell} + \alpha_i(y_j)M_{\text{ref}}]dl_j \qquad (21)$$

where dl_j is the width of the strip, $h_i(y_j)$ and $\alpha_i(y_j)$ are the values of h_i and α_i in the ith mode at y_j in the local coordinate system, and F_{Z_ℓ} and M_{ref} are the force and moment calculated at this strip. The contribution from F_{X_ℓ} to equation (21) is zero since the strip is assumed rigid in the chordwise direction.

Summarizing, the total generalized force from the aerodynamic contribution in each normal mode is calculated as follows: First, the chordwise and normal velocities at any time step are calculated using equation (13). Second, the angle of attack is calculated using equation (14). If the angle of attack is above the section airfoil static stall angle, the lift, drag, and moment coefficients are calculated according to dynamic stall model A. Otherwise, they are obtained from the static airfoil tabular data for this angle of attack. Third, the generalized force on each strip is calculated using equation (21). Finally, the total generalized force on the blade for the ith mode is given by

$$Q_i = \sum_{j=1}^{NS} f_{ij} \qquad i = 1,2,\ldots,NM \qquad (22)$$

where NS is the number of strips (segments) the blade is divided into. This gives the system of equations (eq. 3) for this time step.

Since the governing equations of motion (eq. (3)) are nonlinear in aerodynamics, it is convenient to solve these equations in the time domain. In the present analysis the Wilson-Θ method (ref. 18) is used. This method assumes a linear variation of acceleration between two time steps. The method is an implicit integration method and is unconditionally stable.

The stall response calculation procedure consists of the following steps and is shown schematically in figure 4.

(1) For a given rpm and setting angle, perform a nonlinear finite element analysis, taking into account the geometric stiffness effects due to large deflections. This analysis calculates the steady-state deflections, free-vibration mode shapes, and natural frequencies. For example, a COSMIC-NASTRAN finite element analysis consists of two runs: (a) a NASTRAN solution-4 run to calculate and store the geometric stiffness matrix and steady-state displacements and (b) a NASTRAN solution-9 run using the geometric stiffness matrix generated previously for the frequencies and mode shapes.

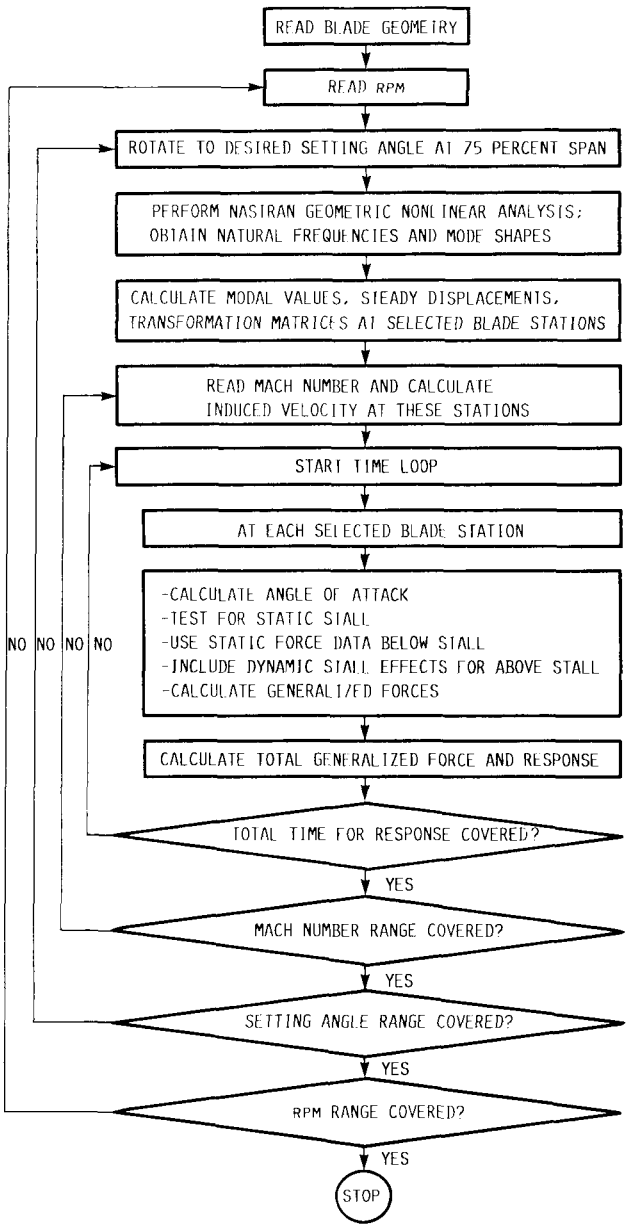

Figure 4.—Flow chart of aeroelastic stall flutter analysis.

(2) Enter the data obtained from step 1 into the ASTROP2 program (ref. 3) to obtain the modal values h_i and α_i and the transformation matrix T_2 relating the basic coordinate system to the local coordinate system at selected radial stations along the blade span. However, for straight blades, using the ASTROP2 program is not necessary since the transformation matrix is a straight-forward, two-dimensional transformation.

(3) Calculate the steady, induced velocity (V_i). In the present study, the combined momentum—blade element theory described in appendix C is used to calculate the induced

velocity. Specifically, the thrust calculated from momentum theory at each radial station is set equal to the thrust produced from the blade airfoil section properties. This procedure gives a nonuniform induced velocity distribution over the disk.

(4) At each strip (segment), calculate the velocity components on the strip, the angle of attack, and the generalized aerodynamic forces (eq. (21)), and obtain the total generalized force (eq. (22)).

(5) Formulate the aeroelastic equations (eq. (3)), and run the stall-flutter code for a response calculation.

(6) For another setting angle or rpm, go back to step 1.

Blade Model and Analysis Description

The SR-2 model propfan has been chosen to demonstrate the capability of the code developed with dynamic stall. Stall-flutter tests have been done for this propfan at zero and low forward speeds (refs. 8 and 9).

The SR-2 propfan model (ref. 19) is designed for an operating condition of Mach 0.8 at a 10.668-km (35 000-ft) altitude, a 243.8-m/s (800-ft/sec) tip speed, and a power loading of 301 kW/m^2 (37.5 shp/ft^2). The model has eight steel blades and is 0.6233 m (2.0416 ft) in diameter D'. The NACA 16 series airfoils are used from the tip to the 45-percent-radius portion of the blade; NACA 65 series airfoils with circular arc (CA) camber lines are used from the 37-percent radius to the root with a transition fairing connecting the two regions. The planform of this model is shown in figure 5. A summary of the pertinent geometric parameters is given in table I and is shown schematically in figure 6. The table shows the distribution of blade geometric twist relative to the geometric twist at 75-percent span $\Delta\beta$, and shows chord c/D', thickness to chord ratio t/c, design lift coefficient c_{ℓ_d}, and airfoil type at 12 stations along the span. In addition, the blade Mach number and angle of attack α will be different at each station depending on the rotational speed, free-stream velocity, and the setting angle.

It can be inferred from the preceding paragraph that for the response calculation one needs a large amount of airfoil data—lift c_ℓ, drag c_d, and moment coefficients $c_{mc/4}$, both in static and dynamic conditions, at several Mach numbers and angles of attack. Reference 14 uses static airfoil data (c_ℓ, c_d, and $c_{mc/4}$) for the SR-2 blade stall-flutter analysis. These static airfoil data are for an isolated blade with no correction for cascade effects. The data are given at five spanwise stations for different Mach numbers and angles of attack; they are interpolated for other stations. However, the accuracy of the static data is not discussed in reference 14. In view of this, to assess the sensitivity of flutter speed for variations in airfoil static data above stall, a parametric investigation was conducted. The results from this investigation are discussed in appendix D.

In the present study, the isolated airfoil static data presented in reference 14 are used since no other static airfoil data are

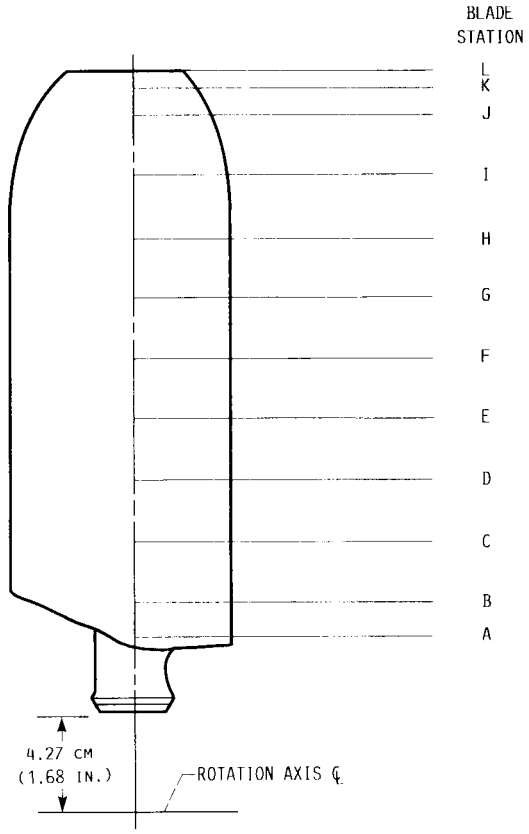

Figure 5.—Planform of SR-2 model propfan blade.

available at this time. The dynamic stall model A is used to calculate response in dynamic conditions. Structural and aerodynamic couplings between blades (i.e, cascade effects) are disregarded. Therefore, a single propfan blade analysis is performed. The material properties used are a Young modulus equal to 30×10^6 psi (206.85 GN/m^2), a Poisson ratio equal to 0.3, and a material density equal to 0.732×10^{-3} lb-sec^2/in^4 (7.823×10^3 kg/m^3).

The experimental data of reference 8 present the variation of total vibratory stress with rpm and indicate that a high stress level, excluding stress levels corresponding to rpm at critical speeds, is an indication of stall flutter or buffeting. (Ref. 8 mentions that buffeting is said to have occurred for blade setting angles above 45°, that buffeting is a multiple mode excitation, and that blade motion has little effect on the loading.) An examination of the data presented in reference 8, indicates that the highest stress levels (taken as indicative of stall flutter) were recorded at about 8500 rpm with a blade setting angle around 30°. This condition is taken as a stall-flutter condition. Therefore for the results presented here most calculations are made for 8500 rpm. However, two more cases, 2000 rpm at a 30° setting angle and 5000 rpm at a 50.3° setting angle, are also analyzed for further validation of the analysis and code. The shaft angle of attack α_s (propeller tilt angle) is taken as zero.

TABLE I.—GEOMETRIC PROPERITES OF SR-2 PROPFAN

[Blade radius, R, 0.311 m (1.0208 ft); number of blades, 8.]

Blade station, (fig. 5)	Non-dimensional[a] y/R	Blade setting angle, $\Delta\beta$, deg	Blade chord c,		Thickness to chord ratio, t/c	Design lift coefficient, $c_{\ell d}$	Airfoil type
			m	ft			
A	0.2392	25.28	0.0872	0.2863	0.212	−0.367	NACA 65 series
B	.2857	18.14	.0884	.2903	.111	−.263	NACA 65 series
C	.3673	12.22	.0908	.2980	.07	−.060	NACA 65 series
D	.449	10.37	.0915	.3004	.045	.075	Transition
E	.5306	7.685	.0907	.2977	.04	.170	Transition
F	.6112	3.88	.0891	.2926	.033	.188	NACA 16 series
G	.6939	1.54	.0881	.2891	.028	.160	↓
H	.7755	−1.05	.0862	.2829	.025	.115	
I	.8571	−3.33	.0822	.2697	.022	.064	
J	.9388	−5.17	.0718	.2357	.021	.025	
K	.9796	−6.31	.0577	.1895	.0205	.01	
L	1.00	−6.87	.0310	.1017	.02	.008	

[a]See figure 3(a).

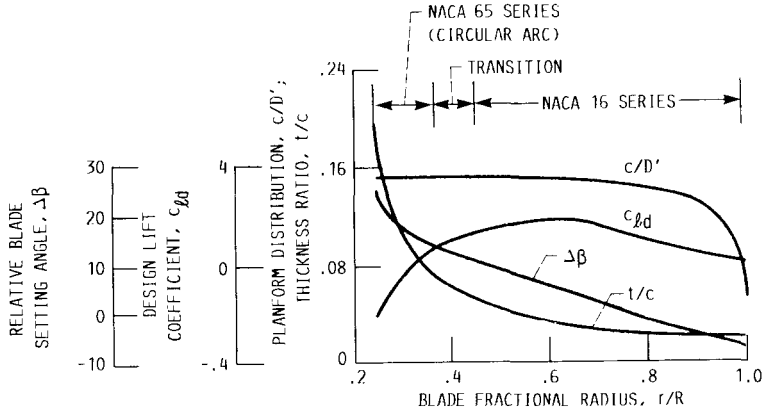

Figure 6.—Variation of propeller design parameters with blade radius for unswept SR-2 propeller.

The mode shapes and natural frequencies were generated using the COSMIC-NASTRAN finite element analysis program using NASTRAN solutions 4 and 9. Triangular elements (CTRIA2) were used for modeling the blade, and the analysis included geometric nonlinear effects due to large deflections. A two-dimensional transformation matrix $[T_2]$ (as given in appendix B) was used to calculate the aerodynamic quantities in the local coordinate system. The reference axis was chosen to be the leading edge. The pitching motion values α_i about this axis were calculated using the translational displacements on the chord line at the strip obtained from the COSMIC-NASTRAN analysis. It should be noted that the transformation matrix $[T_2]$ and the pitching motion values calculated from averaged rotational values at all points on the chord line can also be used (ref. 3). A comparison of pitching motion values calculated from three methods namely, from translational displacements, from average rotational values, and from the nodal values of the COSMIC-NASTRAN analysis at the reference axis point, showed little difference for this blade except near the tip region. However, this may not be true for swept and composite blades.

The first four normal modes were used in the response calculation. The response, variation of the normal coordinates ($q_i s$ in eq. (3)) with time, is plotted for each setting angle at a fixed rpm. A diverging response of any normal coordinate is taken as indication of stall flutter. The response calculations were repeated with different initial conditions (the value of the four normal coordinates, q_1, q_2, q_3, and q_4, at time equal to zero). The response was found to be independent of the initial conditions for the present problem. Therefore in the calculations to follow, the response solution is started with $q_1 = q_2 = q_4 = 0.0$ and $q_3 = 0.01$. The structural damping ratio ζ_i is assumed to be zero unless mentioned specifically. It should be noted here that in reference 8, stresses were plotted with time. Calculation of stresses is beyond the scope of the present study.

Analytical Results and Correlation With Measured Data

This section presents the results of the numerical study performed with the computer code developed.

The first four mode shapes of the blade calculated for 8500 rpm, with the blade setting angle equal to 56.77°, are shown in figure 7. In this case the first two modes were the first and second bending modes, the third mode was the first torsion, and the fourth mode was the third bending mode. Since this was a straight blade with isotropic material properties, the modes were uncoupled. Therefore, the variations of the normal coordinates, q_1, q_2, and q_4 directly represent the variation of bending modes, and the variation of q_3 represents the variation of the first torsion mode. It was found that the untwist due to the centrifugal loads at this rpm is negligible for this blade.

A Campbell diagram (fig. 8) shows the variation of the calculated natural frequencies of the SR-2 propfan with rotational speed at a 56.77° setting angle. Measured frequencies at zero rotational speed are also shown. The first two calculated modal frequencies agree well with the measured values, whereas the third and fourth calculated frequency values show discrepancies of 8.2 and −13.3 percent, respectively, compared with the measured frequencies. The figure also shows straight lines which pass through the origin and express the relationship between the possible exciting frequencies and the rotor speed. The intersection of one of the straight lines with one of the natural frequency curves indicates a potential for resonant vibration near the rotor speed

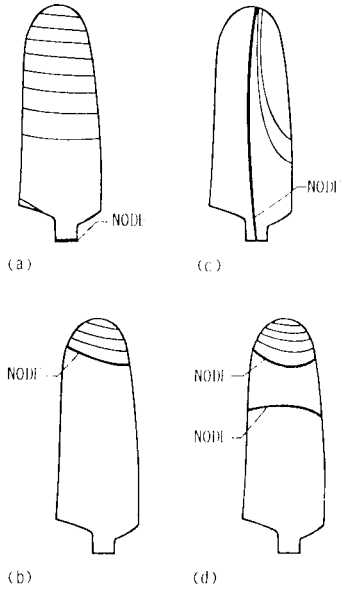

(a) First mode; frequency, 202 Hz.
(b) Second mode; frequency, 513 Hz.
(c) Third mode; frequency, 647 Hz.
(d) Fourth mode; frequency, 870 Hz.

Figure 7.—Calculated mode shape patterns and frequencies for SR-2 propfan blade at 8500 rpm and a blade setting angle, $\beta_{0.75R}$, of 56.77°.

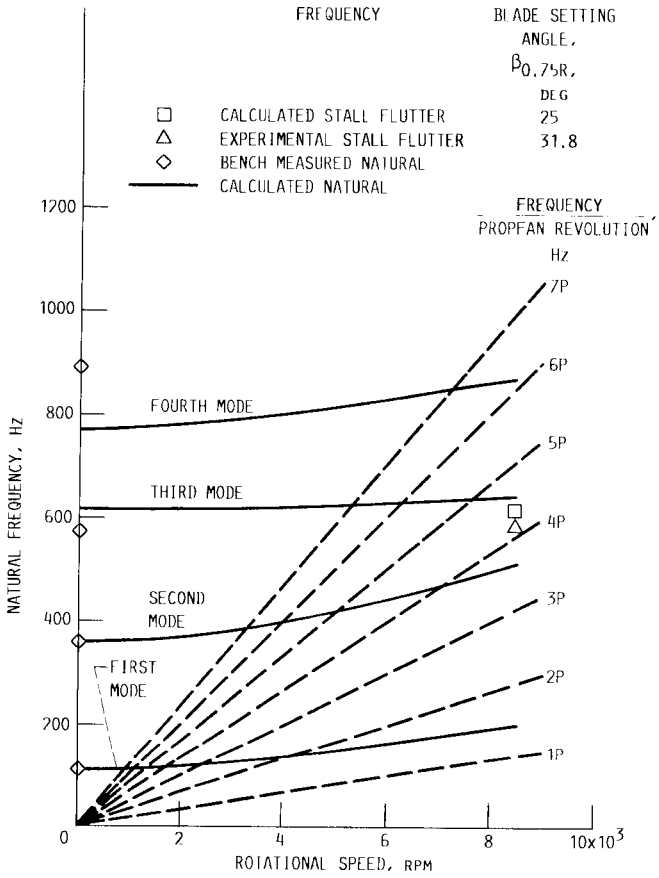

Figure 8.—SR-2 propfan blade natural frequency diagram. Blade setting angle, $\beta_{0.75R}$, 56.77°.

(critical speed) of the intersection point.

Figure 9(a) and (b) shows the response data obtained with dynamic stall model A for a Mach number of 0.169 at a 20° setting angle at 8500 rpm. This condition results in a low angle-of-attack response where dynamic stall effects are zero. The case was run to check the code. It can be seen from these figures that all four modes appear to be converging to a steady value indicating stable oscillations.

Figure 10 shows the response obtained for $M = 0$ and 8500 rpm (i.e., at a static thrust condition). Three blade setting angles were considered: 20°, 25°, and 30°. At these setting angles, the angles of attack were high, resulting in a stalled flow condition. As mentioned earlier, the model A dynamic stall model was used to predict the unsteady forces in stall. Figure 10(a) shows the response of the first normal mode (q_1). The response of this mode appears to be converging to a steady value for all three setting angles. Figure 10(b) shows the response of the third normal mode (q_3). For the 20° setting angle, the motion was stable and approaching a steady value. For the 25° setting angle, the response shows a neutrally stable oscillation. For the setting angle equal to 30° the response was diverging, indicating unstable oscillations. The experimental data presented in reference 8 show that the high vibratory stresses occurred near this setting

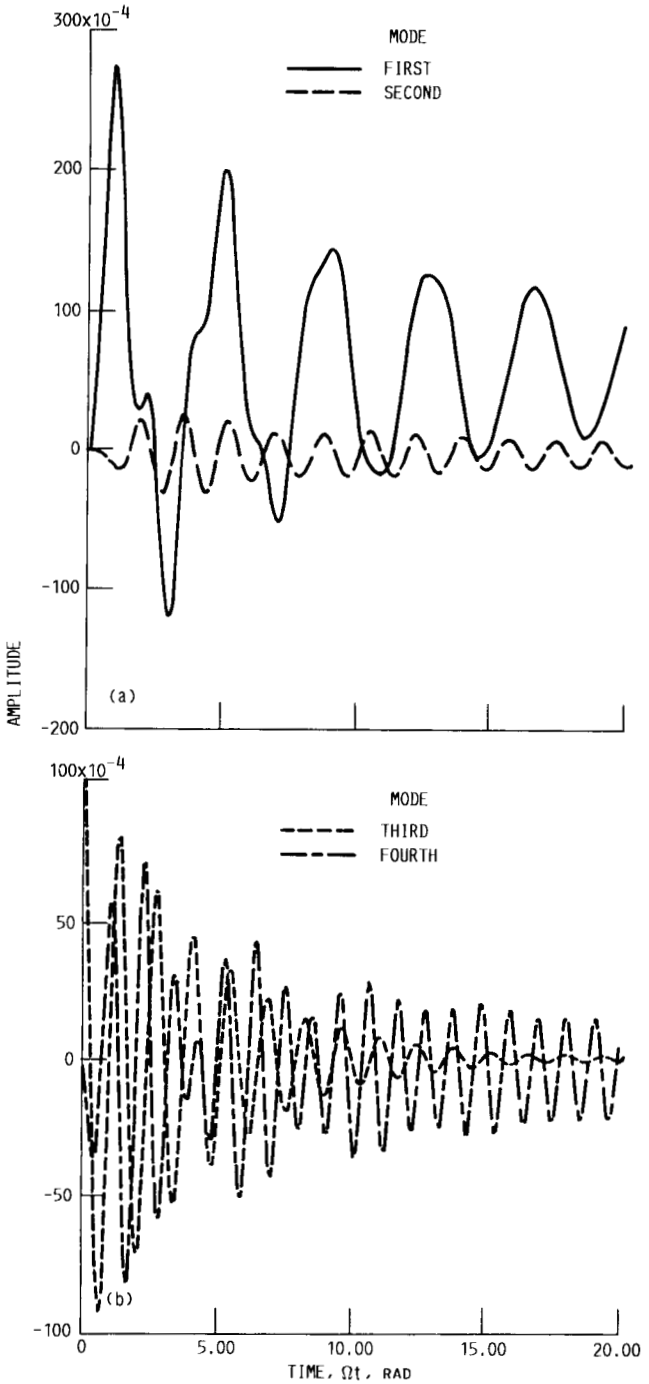

(a) First and second normal mode.
(b) Third and fourth normal mode.

Figure 9.—Response of dynamic stall model A at 8500 rpm, Mach 0.169, and a blade setting angle, $\beta_{0.75R}$, of 20°.

angle (31.8°) and flow condition ($M = 0$). The high stresses are found to not be due to critical speed cross over. The present analysis showed a limit cycle at a 25° setting angle. This condition is taken as a stall flutter condition since the airfoil is at a large initial angle of attack. The calculated frequency of this limit cycle was 617 Hz, which is 3 percent higher than the experimental value of 600 Hz. Note that the calculated value is for zero structural damping. The experimental data of reference 8 show that the large stresses occurred in the third mode (first torsion). The present analysis also predicted that instability occurred in the third normal mode (q_3), which is the first torsion.

Also note that the response trends for the three setting angles are qualitatively in agreement with those that were calculated in reference 14. In reference 14 a beam structural model and model B dynamic stall with unsteady lift and moment data were used in the analysis. Only static drag data were used since unsteady drag data for the NLR–1 airfoil were not available. (A structural damping value of 0.008 was used to see that the response did not diverge at the 30° setting angle.) The

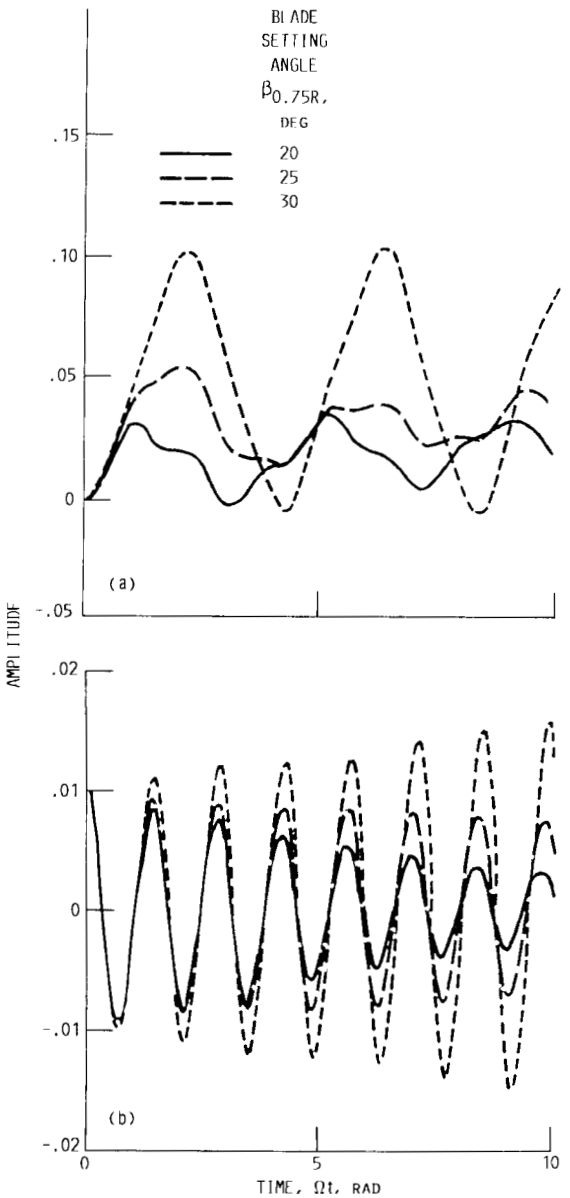

(a) First normal mode.
(b) Third normal mode.

Figure 10.—Response of dynamic stall model A at Mach 0 and 8500 rpm.

agreement between the present study and that in reference 14 is not surprising since for this blade (SR-2) a beam model would have been sufficient because of zero sweep and isotropic material properties. However, as mentioned earlier, a finite element formulation is more general and applicable to swept propfans made of composite materials. Also the unsteady drag effects on the response were minimized since the chord was assumed rigid and only a fraction of drag contributed to the normal force on the airfoil.

It is interesting to determine if the stall flutter that occurred was essentially a single-degree-of-freedom flutter (third mode—first torsion). To verify this, the stall-flutter response code was run with only one mode included, and the response calculation was repeated at a 30° setting angle. The study showed that with only the third mode included in the analysis the response was diverging, while the response with each of the other modes was converging. This shows that for this blade and flow condition, the analysis predicted that the stall flutter is essentially a single-degree-of-freedom flutter. The calculations of reference 8 also showed that all the instabilities were third mode instabilities and that no instabilities were calculated for the first and second modes.

A response calculation was also performed at 2000 rpm with a blade setting angle of 30°. All four modes showed a converging trend as shown in figure 11, indicating stable oscillations. The experimental data also showed a low stress value indicating stable oscillations. It may be noted that the previous analytical study showed instability at this setting angle and 8500 rpm.

Further verification of the present analysis is given in figure 12. The flow conditions were 5000 rpm at a 50.3° setting angle with zero forward speed. The spectral plot of the measured stress (ref. 8) shows that the response is substantially in the first mode. Reference 8 states that "this may be a buffet condition exciting the first mode with some $2p$ magnification (a frequency of 2 Hz per propfan revolution) due to the nearness of the $2p$ critical speed." The behavior shown in

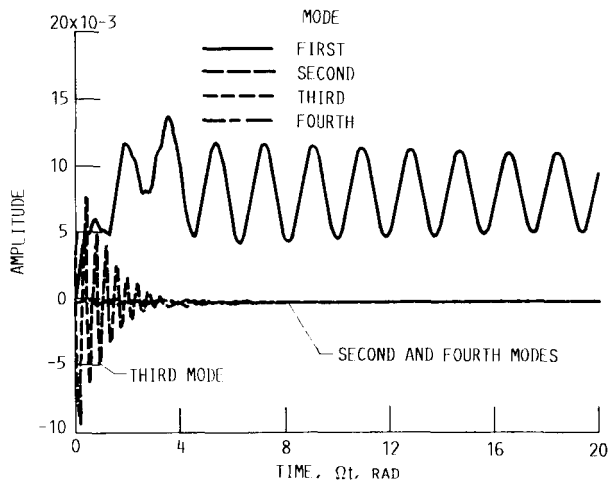

Figure 11.—Response of four modes at 2000 rpm, Mach 0, and a blade setting angle, $\beta_{0.75R}$, of 30°.

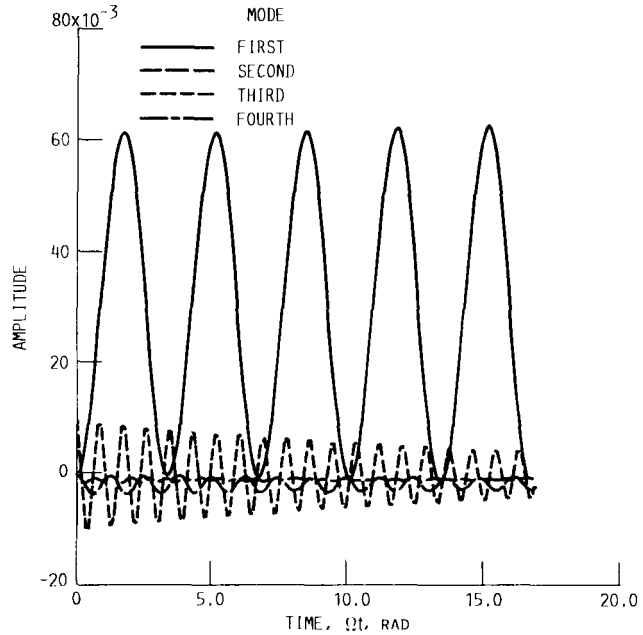

Figure 12.—Response of four modes at 5000 rpm, Mach 0, and a blade setting angle, $\beta_{0.75R}$, of 50.3°.

figure 12 is predicted in the analysis. All the modes except the first mode show a converging trend, indicating high stresses in the first mode. This further validates the present code and the analysis.

In figure 13(a) and (b) the response data obtained from dynamic stall models A and B are compared. The response was calculated for a Mach number of zero and a setting angle of 20°. The response of the first and third normal coordinates, respectively, are shown. Both modes show a definite converging trend with both models. Also, the second and fourth modes (not shown here) showed a converging trend indicating stable oscillations. Even though the unsteady drag effects are included in model A, but not included in model B, both models show a close qualitative trend in the response. This confirms that the contribution of drag is minimum in this case.

To calculate the maximum value of the setting angle for which the blade is unstable in the static thrust condition, the response data for different setting angles is needed. Figure 14 shows the damping values calculated from the response curves of the third mode as a function of setting angle, obtained with dynamic stall models A and B at 8500 rpm. As expected, model B predicted a slightly higher setting value (thereby, a higher angle of attack), before it predicted unstable oscillations compared to model A. However, for setting angles higher than 30°, the flow might have completely separated with no reattachment (deep stall), and the application of the dynamic stall models (A and B) is restricted.

Discussion on the Calculations

Even though the present analysis predicted the mode and the setting angle for the stall flutter onset as per the experiment, the following comments are in order:

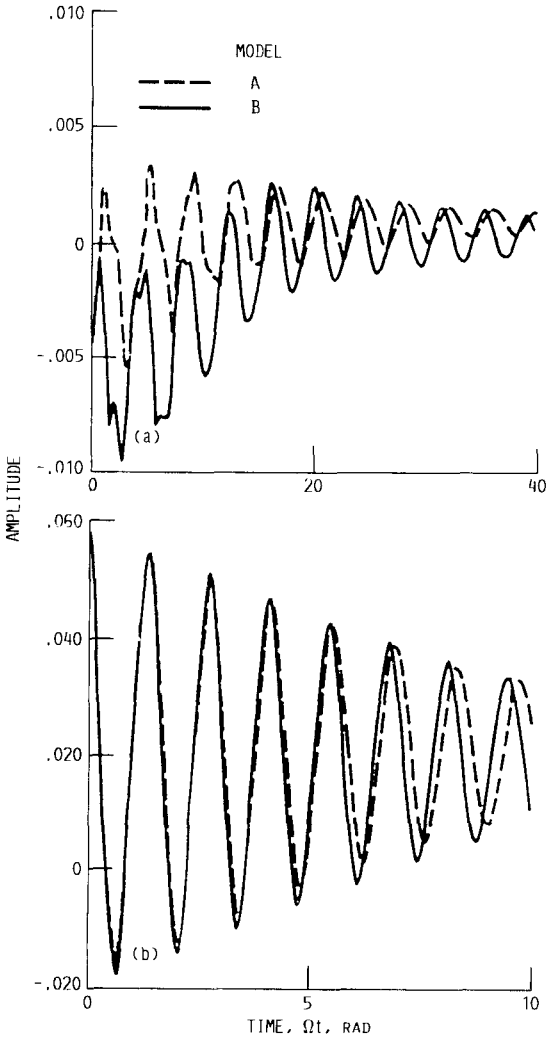

(a) First normal mode.
(b) Third normal mode.

Figure 13.—Response of models A and B at 8500 rpm, Mach 0, and a blade setting angle, $\beta_{0.75R}$, of 20°.

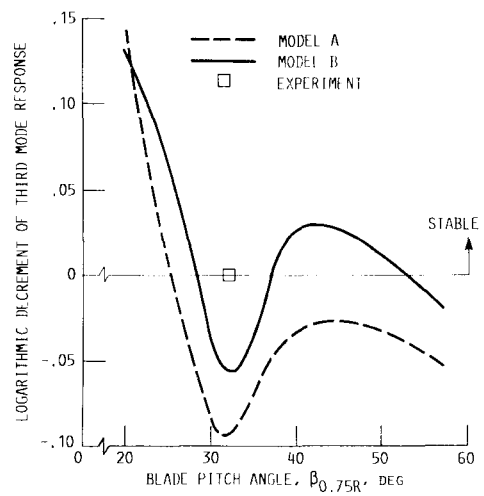

Figure 14.—Variation of logarithmic decrement with setting angle at 8500 rpm and Mach 0.

(1) Test data evaluated in reference 8 do not show the stress levels at all gages for the same setting angle. Hence, it was difficult to assess whether there was multimode excitation indicating buffeting. However test data evaluated at NASA Lewis for the same case as in reference 8 showed higher stresses both at the tip bending gage and at the shear gage for the same flow conditions, indicating a multimodal excitation for the SR-2 blade.

(2) Experimental data showed that the instability moved from a third mode to a second mode instability at higher angles of attack, a phenomena which was not predicted by the present analysis. All the modes showed instability at higher angles.

(3) The validity of the present aerodynamic model at angles of attack where buffet is assumed to have occurred has yet to be investigated.

Conclusions

The stall flutter response of an unswept SR-2 propfan wind-tunnel model was studied with a semiempirical dynamic stall model. The results were compared with available experimental and analytical data. The following conclusions are drawn from this study.

1. The Gormont dynamic stall model (model A), where only a correction to angle of attack is used, qualitatively predicts the same trend as that observed in experiments. The predictions of this model agree well with those predicted by the Gangwani dynamic stall model (model B), a model based on the synthesization procedure.

2. Both models are conservative in predicting the setting angle at which stall-flutter occurred in the experiment.

3. Even though the present study and that of reference 14, where a beam model is used, predicted the same behavior; a finite element formulation is more general, particularly for applications to swept propfan blades with composite materials.

The following suggestions are made to improve the analysis:

1. Experimental static and dynamic stall data for NACA 16 series airfoils that are employed for propfans should be generated and used in the analysis.

2. Cascade corrections to isolated airfoil lift, drag, and moment coefficients should be included.

3. A more refined induced velocity calculation method is required especially at static thrust conditions.

4. For a more direct comparison with experimental data, a stress calculation module should be developed and included in the code.

5. The formulation and the computer code should be checked for swept blades and should be applied to study the response with blades made up of composite materials.

6. The analysis should include a complete nonlinear analysis both in structural modeling and aerodynamic modeling instead of a linearized structural model and nonlinear aerodynamic model as was done here.

Appendix A
Symbols

A	disk area
A_i, B_i	points on the reference line
a	distance between reference axis and the quarter chord
a_{01}	static lift curve slope
B	number of blades
b	semichord
c	full chord
$\hat{c}, \hat{t}, \hat{n}$	unit vectors along the X_ℓ, Y_ℓ, Z_ℓ axes
c_d	aerodynamic drag coefficient
c_ℓ	aerodynamic lift coefficient
$c_{\ell d}$	design lift coefficient
c_m	aerodynamic moment coefficient about the reference axis
$c_{mc/4}$	aerodynamic moment coefficient about the quarter chord
D	drag
D'	diameter of the propfan
d	distance between the reference axis and the three-quarter chord
dl_j, dr	width of the strip
F_{X_ℓ}	force component in the X_ℓ direction (eq. (20))
F_{Z_ℓ}	force component in the Z_ℓ direction (eq. (20))
f_{ij}	generalized force at the jth strip
h	plunging degree of motion, positive downward
h_i	contribution of ith modal deflection to plunging motion
$\hat{i}, \hat{j}, \hat{k}$	unit vectors along the X_B, Y_B, Z_B axes
K_1	unsteady aerodynamic empirical factor (eq. (17))
k	reduced frequency based on semichord
L	aerodynamic lift force
M	Mach number
M_a	aerodynamic moment
M_{ref}	moment about the reference axis (eq. (20))
m_i	generalized mass in the ith normal coordinate
NM	number of normal modes
NS	number of blade segments
n	rotor speed in revolutions per second
$\hat{n}$	normal vector
np	frequency of n Hz per propfan revolution
Q_i	generalized aerodynamic force in the ith normal coordinate
q_i	ith generalized (normal) coordinate
R	rotor radius
Re	Reynold number
r	position of a mass point (eq. (7))
$sign\ (\ )$	sign of ( ), either positive or negative
T	thrust
$[T_1], [T_2]$	transformation matrices
t	time
t/c	airfoil thickness to chord ratio
U_c, U_t, U_n	chordwise, tangential, and normal velocities at a section
u, v, w	unsteady (perturbed) displacements at a point
u_0, v_0, w_0	steady displacements at a point
V_i	steady induced velocity
V_R	resultant velocity, $\sqrt{U_c^2 + U_n^2}$
V_{rel}	relative velocity vector
V_∞	free-stream velocity
X_B, Y_B, Z_B	basic (rotating) coordinate system
X_I, Y_I, Z_I	inertial coordinate system
X_ℓ, Y_ℓ, Z_ℓ	local coordinate system
x, y, z	coordinates of a point in the basic coordinate system
y_j	y coordinate of jth strip
α	instantaneous angle of attack
$\alpha_{c_\ell=0}$	angle of attack for zero lift
α_E	effective angle of attack (eq. (16)).
$\alpha_{E,L}$	effective angle of attack for lift (eq. (18)).
α_i	contribution of ith modal deflection to pitching motion
α_p	pitching degree of motion, positive (nose up)
α_s	shaft (propeller tilt) angle of attack
α_{ss}	static stall angle
α_0	mean or initial angle of attack
$\bar{\alpha}$	amplitude of oscilliation
$\beta_{0.75R}$	blade pitch setting angle at 0.75 radius
$\Delta\beta$	setting angle relative to the one at 0.75 radius
γ	stall delay function (eq. (19))
$\Delta\alpha_{DS}$	incremental dynamic stall angle (eq. (15))
ζ_i	critical damping (structural) ratio in the ith mode
ρ_a	air density

ϕ	inflow angle
ψ	Ωt, nondimensional time
Ω	blade rotational speed, rad/sec
ω_i	coupled frequency in the ith mode
$\bar{\omega}$	rotational vector (eq. (5))
$\partial(\ )/\partial y$	derivative with respect to y in the local coordinate system
$(\dot{})$	$d(\ )/dt$
$(\ddot{})$	$d^2(\ )/dt^2$

Subscripts:

a	airflow
B	basic
b	blade
I	inertial
L	lift
ℓ	local
M	moment
m	due to blade motion
rel	relative
rot	due to blade rotation
s	steady

Superscripts:

T	transpose
$-$	vector
$\hat{}$	unit vector

Appendix B
Calculation of Unit Vectors

This appendix presents the calculation of unit vectors of the X_ℓ, Y_ℓ, Z_ℓ coordinate system, and thereby the calculation of the transformation matrix, $[T_2]$, relating the basic coordinate system to the local coordinate system.

Let $A_i(x,y,z)$ represent points on the reference line, where the unit vectors are to be calculated. The index i ranges from 1 to the number of strips the blade is divided into. Consider another adjacent point $A_{i+1}(x + \Delta x, y + \Delta y, z + \Delta z)$.

The unit vector $\hat{t}$, tangent to the reference line at the point A_i and positive from root to tip, is given approximately as

$$\hat{t}_i = \frac{A_{i+1} - A_i}{\Delta s} = t_{1i}\hat{i} + t_{2i}\hat{j} + t_{3i}\hat{k} \tag{B1}$$

where

$$\Delta s = \sqrt{(\Delta x)^2 + (\Delta y)^2 + (\Delta z)^2} \tag{B2}$$

and $\hat{i}$, $\hat{j}$, and $\hat{k}$ are the unit vectors in the basic coordinate system.

The chord line vector $\hat{c}$ is a line that lies in a plane perpendicular to the tangent vector $\hat{t}$. Let this plane intersect the trailing edge line of the blade at point B_i. The direction of $\hat{c}$ is obtained by joining points A_i and B_i directed towards B_i. The unit vector $\hat{c}$ is given by

$$\hat{c}_i = \frac{B_i - A_i}{|B_i - A_i|} = c_{1i}\hat{i} + c_{2i}\hat{j} + c_{3i}\hat{k} \tag{B3}$$

Then the normal vector $\hat{n}$ at point A_i is given by the cross product of vectors $\hat{c}$ and $\hat{t}$: that is,

$$\hat{n} = \hat{c} \times \hat{t} \tag{B4}$$

This procedure of finding the transformation matrix between the local and the basic coordinate systems automatically accounts for the curvature of the reference axis. Summarizing, the chordwise, tangent, and normal unit vectors at any point A_i are given by

$$\begin{Bmatrix} \hat{c} \\ \hat{t} \\ \hat{n} \end{Bmatrix} = \begin{bmatrix} c_1 & c_2 & c_3 \\ t_1 & t_2 & t_3 \\ n_1 & n_2 & n_3 \end{bmatrix} \begin{Bmatrix} \hat{i} \\ \hat{j} \\ \hat{k} \end{Bmatrix} \tag{B5}$$

Then the transformation between the local and basic coordinate system is given by

$$\begin{Bmatrix} X \\ Y \\ Z \end{Bmatrix}_B = \begin{bmatrix} c_1 & t_1 & n_1 \\ c_2 & t_2 & n_2 \\ c_3 & t_3 & n_3 \end{bmatrix} \begin{Bmatrix} X \\ Y \\ Z \end{Bmatrix}_\ell \tag{B6}$$

or

$$\{X\}_B = [T_2]\{X\}_\ell \tag{B7}$$

Appendix C
Calculation of Steady Induced Velocity

This appendix presents the equations to calculate steady induced velocity V_i (see eq. (4)) using the combined momentum—blade element theory. A discussion on other methods of calculating induced velocity is also included.

In momentum theory, the propfan is approximated by an infinitely thin actuator disk across which the static pressure increases discontinuously. The assumptions inherent in this model (ref. 20) are (1) the velocity is constant through the disk, (2) the pressure is uniform over the disk, (3) rotation imparted to the flow as it passes through the propfan is neglected, (4) the flow passing through the propfan can be separated from the rest of the flow by a well-defined stream tube, and (5) the flow is incompressible. Applying the Bernoulli equation ahead and downstream of the propfan, it can be shown that the thrust is given by

$$T = \rho_a A(V_\infty \cos \alpha_s + V_i)2V_i \tag{C1}$$

where V_∞ is the free-stream velocity, V_i is the induced velocity, ρ_a is the air density, A is the disk area, and α_s is the shaft angle of attack. This can be interpreted as thrust equal to mass flux through the propfan, $\rho_a A\ (V_\infty \cos \alpha_s + V_i)$, times the total increase in the velocity of the flow $(2V_i)$.

The thrust produced by the propfan can also be calculated from the known aerodynamic properties (c_ℓ and c_d) of the propfan blade. Figure 15 shows the cross section of a blade with velocities influencing the element. The pitch angle β, of the section is defined relative to the zero lift line of the airfoil section. The contribution of one blade element to the thrust T is

$$dT = dL \cos(\phi + \alpha_i) - dD \sin(\phi + \alpha_i) \tag{C2}$$

where dL and dD are the differential lift and drag forces, respectively, and α_i is the induced angle of attack due to the induced velocity V_i. The lift and drag forces, dL and dD, are given by

$$dL = \frac{1}{2}\rho_a V_R^2 c(c_\ell)\, dr$$

$$dD = \frac{1}{2}\rho_a V_R^2 c(c_\ell)\, dr \tag{C3}$$

Here c_ℓ is given by $a_{01}(\beta - \phi - \alpha_i)$, where a_{01} is the linear lift curve slope, c_d can be obtained as a function of c_ℓ, and c is the chord.

Assuming α_i and drag to lift ratio to be small, dT for B number of blades is given by

$$dT = \frac{1}{2} B\rho_a V_R^2 c(a_{01})(\beta - \phi - \alpha_i) \cos(\phi - \alpha_i)\, dr \tag{C4}$$

By applying equation (C1) to the differential annulus, the elemental thrust is given by

$$dT = (2\pi r\, dr)(V_\infty \cos\alpha_s + V_i \cos\alpha_i)2V_i \cos\alpha_i \tag{C5}$$

Equating equation (C4) to (C5) yields a quadratic equation for V_i, from which V_i can be calculated.

Note that other blade element theories differ from the momentum—blade element theory principally in the way in which the wakes are modeled. The basic vortex theory describes the wake by a series of cylindrical vortex sheets representing the radial variation of circulation, implying an infinite number of blades.

Goldstein (ref. 21) assumes helecoidal surfaces for each blade. The helecoids are assumed to move downward uniformly at the average momentum velocity, and the effects of wake contraction, viscosity, and nonuniform downwash on the wake shape are neglected. This theory is inadequate when used to analyze propfans with increased blade loading, tip Mach number, and number of blades. Also this method is inadequate to predict static (static thrust condition) performance where wake contraction and tip rollup must be taken into account. Wake contraction will position the vortex generated by each blade tip closer to the tip path plane than is assumed in the Goldstein analysis. Close proximity of the tip vortex to the following blades causes severe local inflow distribution due to high rotational velocities with the vortex. These rotational velocities reach levels as high as 50 percent of the blade tip speed.

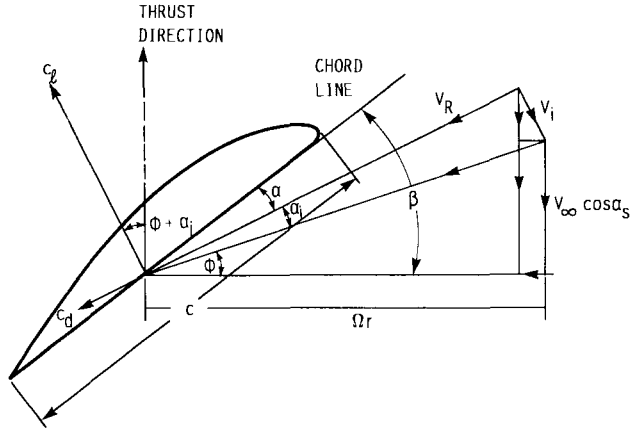

Figure 15.—Velocity and force diagram for propeller blade element.

Various methods—namely, lifting line, lifting surface, vortex lattice method (VLM), and computational fluid dynamics (CFD)—have developed to account for wake geometry and wake distortion for low- to high-speed flights. For static thrust conditions, either a prescribed wake geometry from experimental observation is used in the analysis or the induced velocity extrapolated from low-speed flight analysis is used. (See refs. 21 to 24 for further details.) These methods can be used for swept propfans. When applying combined momentum—blade element theory, the blade sections have to be taken along the streamline.

Appendix D
Effect of Airfoil Static Data Variation on the Dynamic Stall Response

To understand the effect of airfoil static data above stall on the stall-flutter response, one can make calculations with prescribed static data above stall, and the variation in response can be studied. However, for a response study, c_f, $c_{mc/4}$, and c_d cannot be varied independently since they are interrelated. However, dynamic stall loops (dynamic lift, moment, and drag versus angle of attack) can be obtained with independent variation of static lift, drag, and moment coefficients above stall, and some inference can be drawn. In stall flutter, the negative aerodynamic damping is mostly from the dynamic moment loop. So in the present study the static $c_{mc/4}$ is varied and the dynamic moment loops are studied. Three cases are studied as shown below and in figure 16.

Case-A Moment Coefficient

This case is a curve-fitted expression for the static moment data given in the G400PROP program (ref. 14) at the 75-percent-radius location for a Mach number of 0.7,

$$c_{mc/4} = -0.035 - 0.003^{*}\alpha \qquad \text{for } \alpha < 6^{\circ}$$

$$c_{mc/4} = -0.053 - 0.024^{*}(\alpha - 6.0) \qquad \text{for } 6^{\circ} < \alpha < 10^{\circ}$$

$$c_{cm/4} = -0.149 - 0.0085^{*}(\alpha - 10) \qquad \text{for } \alpha > 10^{\circ}$$

Case-B Moment Coefficient

$$c_{mc/4} = -0.553 - 0.015(\alpha - 6) \qquad \text{for } \alpha > 6^{\circ}$$

Case-C Moment Coefficient

$$c_{mc/4} = -0.553 - 0.010(\alpha - 6) \qquad \text{for } \alpha > 6^{\circ}$$

Figure 17 shows the dynamic $c_{mc/4}$ loops obtained with static-stall moment data assumed as above. The angle-of-attack variation is given by $\alpha = 5^{\circ} + 3^{\circ}\sin(\omega t)$ at a reduced frequency of 0.05 and for a Mach number of 0.7. The dynamic loops are indicative of the energy transfer from the flow to the structure. In figure 17, the dynamic loop obtained with case-A static data shows a large hysteresis loop above stall, which means that negative work is being done on the structure. This may lead to a net negative damping at certain flow conditions. The area of the loop reduces by about half with case-B assumed static data. With the case-C assumed static data no negative loop is obtained, indicating there is no negative work on the structure. This shows that inaccurate static data above stall can lead to positive or negative damping, leading to stable or unstable response.

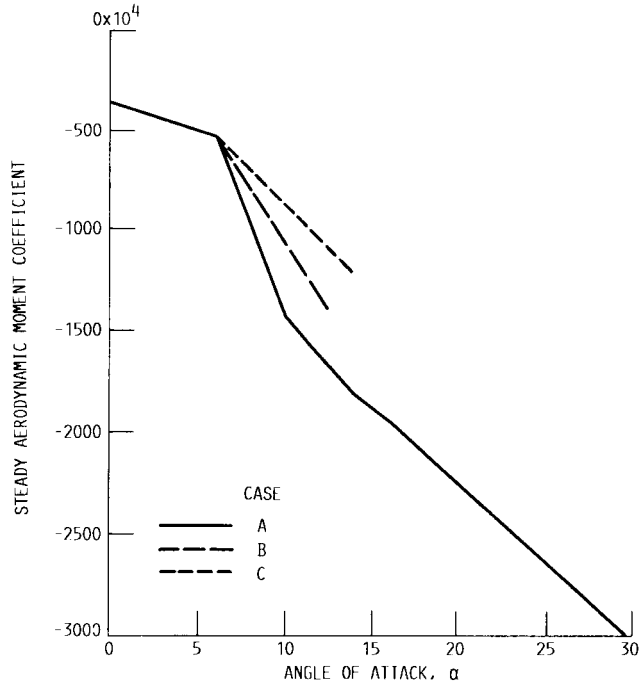

Figure 16.—Variation of static moment coefficient with angle of attack.

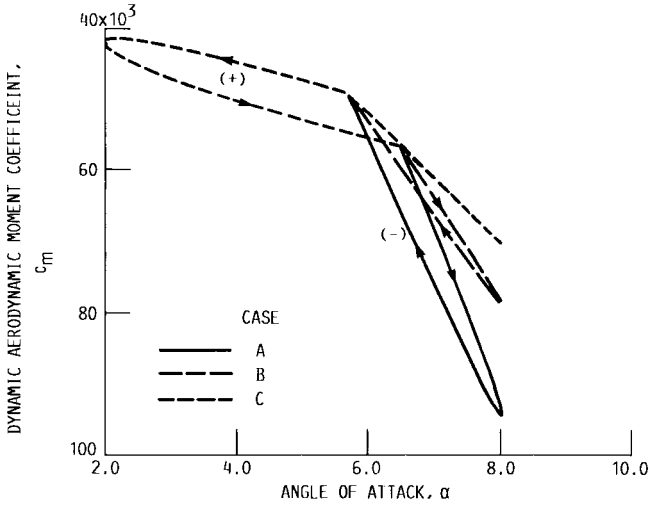

Figure 17.—Variation of dynamic moment coefficient with assumed static moment coefficient at Mach 0.7 and reduced frequency, k, of 0.05; $\alpha = 5 + 3 \sin ks$; model A dynamic stall.

References

1. Mehmed, O., et al.: Bending-Torsion Flutter of a Highly Swept Advanced Turboprop. NASA TM-82975, 1981.
2. Mehmed, O.; and Kaza, K.R.V.: Experimental Classical Flutter Results of a Composite Advanced Turboprop Model. NASA TM-88792, 1986.
3. Kaza, K.R.V., et al.: Analytical Flutter Investigation of a Composite Propfan Model. 28th Structures, Structural Dynamics and Materials Conference, Part 2A, AIAA, 1987, pp. 84-97. (NASA TM-88944).
4. Kaza, K.R.V., et al.: Analytical and Experimental Investigation of Mistuning in Propfan Flutter. 28th Structures, Structural Dynamics and Materials Conference, Part 2A, AIAA, 1987, pp. 98-110. (NASA TM-88959).
5. Reddy, T.S.R; and Kaza, K.R.V.: A Comparative Study of Some Dynamic Stall Models. NASA TM-88917, 1987.
6. McCroskey, W.J.: The Phenomenon of Dynamic Stall. NASA TM-81264, 1981.
7. Galbraith, R.A.M; and Vezza, M: Methods of Predicting Dynamic Stall. Wind Energy Conversion 1986, R.A.M. Galbraith, et al., eds., Mechanical Engineering Publications, London, 1986, pp. 263-272.
8. Smith, A.F.: Analysis and Test Evaluation of the Dynamic Stability of Three Advanced Turboprop Models at Zero Forward Speed. (HSER-11054, Hamilton Standard; NASA Contract NAS3-22755) NASA CR-175025, 1985.
9. Smith, A.F.: Analysis and Test Evaluation of the Dynamic Response and Stability of Three Advanced Turboprop Models at Low Forward Speed. (HSER-11055, Hamilton Standard; NASA Contract NAS3-22755) NASA CR-175026, 1985.
10. Gormont, R.E.: A Mathematical Model of Unsteady Aerodynamics and Radial Flow for Application to Helicopter Rotors. USAAMRDL-TR-72-67, May 1973. (Avail. NTIS, AD-767240).
11. Gangwani, S.T.: Synthesized Airfoil Data Method for Prediction of Dynamic Stall and Unsteady Airloads. NASA CR-3672, 1983. (Also see; Prediction of Dynamic Stall and Unsteady Airloads for Rotor Blades. J. Am. Helicopter Soc., vol. 27, no. 4, Oct. 1982, pp. 57-64).
12. Tran, C.T.; and Petot, D.: Semi-Empirical Model for the Dynamic Stall of Airfoils in View of the Application to the Calculation of Responses of a Helicopter Blade in Forward Flight. Vertica, vol. 5, no. 1, 1981, pp. 35-53.
13. Steinman, D.B.: Aerodynamic Theory of Bridge Oscillations. Proc. Am. Soc. Civ. Eng., vol. 75, no. 8, Oct. 1949, pp. 1147-1184.
14. Bielawa, R.L., et al.: Aeroelastic Analysis of Propellers. NASA CR-3729, 1983.
15. Bisplinghoff, R.L.; Ashley, H.; and Halfman, R.L.: Aeroelasticity. Addison-Wesley Publishing Co., 1955, pp. 397-398.
16. Egolf, T.A., et al.: An Analysis for High Speed Propeller-Nacelle Aerodynamic Performance, Vol. 1—Theory and Initial Application; Vol. 2—User's Manual for the Computer Program. (R79-912949-19, United Technologies Research Center; NASA Contract NAS3-20961) NASA CR-169450, NASA CR-169451, 1979.
17. Maksymiuk, C.M; and Watson, S.A.: A Computer Program for Estimating the Aerodynamic Characteristics of NACA 16-Series Airfoils. NASA TM-85696, 1983.
18. Bathe, K.J.; and Wilson, E.L.: Numerical Methods in Finite Element Methods. Prentice Hall, 1976.
19. Stefko, G.L.; and Jeracki, R.J.: Wind Tunnel Results of Advanced High Speed Propellers in the Takeoff, Climb, and Landing Operating Regimes. AIAA Paper 85-1259, July 1985. (NASA TM-87054).
20. McCormick, B.W.: Aerodynamics, Aeronautics, and Flight Mechanics. John Wiley & Sons, 1979, pp. 343-369.
21. Goldstein, S.: On the Vortex Theory of Screw Propellers. Proc. R. Soc. London Ser. A, vol. 123, no. 792, Apr. 6, 1929, pp. 440-465.
22. Miller, C.J.: Optimally Designed Propellers Constrained by Noise. Ph.D. Thesis, Purdue University, 1984.
23. Williams, M.H.; and Huang, C.C.: Three Dimensional Unsteady Aerodynamics and Aeroelastic Response of Advanced Turboprops. 27th Structures, Structural Dynamics and Materials Conference, Part 2, AIAA, 1986, pp. 116-124.
24. Bober, L.J. ; Chaussee, D.S.; and Kutler, P.: Prediction of High Speed Propeller Flow Fields Using a Three Dimensional Euler Analysis. AIAA Paper 83-0188, Jan. 1983. (NASA TM-83065).

NASA
National Aeronautics and Space Administration

Report Documentation Page

1. Report No.	2. Government Accession No.	3. Recipient's Catalog No.
NASA TM-4083		

4. Title and Subtitle
Analysis of an Unswept Propfan Blade With a Semiempirical Dynamic Stall Model

5. Report Date
January 1989

6. Performing Organization Code

7. Author(s)
T.S.R. Reddy and K.R.V. Kaza

8. Performing Organization Report No.
E-4196

10. Work Unit No.
535-03-01

9. Performing Organization Name and Address
National Aeronautics and Space Administration
Lewis Research Center
Cleveland, Ohio 44135-3191

11. Contract or Grant No.

13. Type of Report and Period Covered
Technical Memorandum

12. Sponsoring Agency Name and Address
National Aeronautics and Space Administration
Washington, D.C. 20546-0001

14. Sponsoring Agency Code

15. Supplementary Notes
T.S.R. Reddy, The University of Toledo, Department of Mechanical Engineering, Toledo, Ohio 43606 and NASA Resident Research Associate; K.R.V. Kaza, NASA Lewis Research Center.

16. Abstract
The time-history response of a propfan wind-tunnel model with dynamic stall was studied analytically. The response obtained from the analysis was compared with available experimental data. The governing equations of motion were formulated in terms of blade normal modes calculated using the COSMIC-NASTRAN computer code. The response analysis considered the blade plunging and pitching motions. The lift, drag, and moment coefficients for angles of attack below the static stall angle were obtained from a quasi-steady theory. For angles above static stall angles, a semiempirical dynamic stall model based on a correction to the angle of attack was used to obtain lift, drag, and moment coefficients. Using these coefficients, the aerodynamic forces were calculated at a selected number of strips, and integrated to obtain the total generalized forces. The combined momentum—blade element theory was used to calculate the induced velocity. The semiempirical stall model predicted a limit cycle oscillation near the setting angle at which large vibratory stresses were observed in an experiment. The predicted mode and frequency of oscillation also agreed with those measured in the experiment near this setting angle. The results also correlated well with the other published data that used a semiempirical dynamic stall model based on a synthesized procedure.

17. Key Words (Suggested by Author(s))	18. Distribution Statement
Propfans; Flutter; Dynamic stall; Stall flutter; Empirical models	Unclassified – Unlimited Subject Category 01

19. Security Classif. (of this report)	20. Security Classif. (of this page)	21. No of pages	22. Price*
Unclassified	Unclassified	22	A03

NASA FORM 1626 OCT 86

*For sale by the National Technical Information Service, Springfield, Virginia 22161